PAPER

Check for updates

High performance and insensitive energetic compounds from the intelligent assembly of nitramino/*gem*-dinitromethyl group and oxadiazoles

Fangming Chen,†[a] Qiong Yu, [ID] †*[a] Zihao Guo, [ID] [a] Kejia Peng,[ab] Wenjie Zhou,[a] Wenbin Yi, [ID] *[a] Richard J. Staples [ID] [c] and Jean'ne M. Shreeve [ID] *[d]

It is widely recognized that an increase in the number of *gem*-dinitromethyl or nitamino groups in compounds typically leads to a higher oxygen balance and enhanced performance, but at the cost of reduced molecular stability. In order to effectively balance high-performance and mechanical sensitivity, the intelligent assembly of energetic groups and backbones has been identified as a promising strategy. Here, the combination of nitramino, *gem*-dinitromethyl groups and oxadiazoles gave 4-nitramino-3-(5-dinitromethyl-1,3,4-oxadiazole)-1,2,5-oxadiazole (**8**) and its corresponding four energetic salts. Furthermore, it is worth noting that the exact structural features of compounds **3** and **6** were successfully validated using single crystal diffraction data. Neutral compound **8** showed a commendable oxygen balance of 10.6%, as well as excellent detonation velocity of 8808 m s^{-1} and detonation pressure of 34.2 GPa. The dihydroxylammonium salt **6** and dihydrazinium salt **7** demonstrated exceptional detonation properties (**6**: 8762 m s^{-1}, 33.6 GPa; **7**: 8800 m s^{-1}, 33.1 GPa) and outstanding sensitivities (IS > 40 J, FS > 360 N), indicating their high potential as a replacement for RDX (8795 m s^{-1}, 34.9 GPa, 7.4 J, 240 N).

Introduction

The past few decades have seen substantial acceleration in research concerning high-energy density materials (HEDMs).[1–4] The pursuit of these materials has led to the discovery of various nitrogen-containing compounds, each with unique and promising properties.[5] The strategic modification of nitrogen-rich heterocyclic frameworks with explosophoric groups has indeed been recognized as a highly effective approach for synthesizing high-performance energetic compounds. This approach leverages the unique properties of nitrogen-rich heterocyclic frameworks, which provide a robust structural basis for incorporating and stabilizing explosophoric groups. By carefully selecting and positioning these groups within the framework, it is possible to create energetic compounds with enhanced performance characteristics, such as higher density, faster burning rate, and improved safety.

[a] *School of Chemistry and Chemical Engineering, Nanjing University of Science and Technology, Nanjing 210094, China. E-mail: qyu@njust.edu.cn, yiwb@njust.edu.cn*

[b] *Mendeleev University of Chemical Technology of Russia, Moscow, 125047, Russia*

[c] *Department of Chemistry, Michigan State University, East Lansing, Michigan 48824, USA*

[d] *Department of Chemistry, University of Idaho, Moscow, Idaho 83844-2343, USA. E-mail: jshreeve@uidaho.edu*

† Fangming Chen and Qiong Yu contributed equally to this work.

The framework usually chosen for heterocyclic rings containing nitrogen or oxygen is typically a five- or six-membered ring. The most common examples of these rings are tetrazine, tetrazole, triazole, pyrazole and oxadiazole. In five-membered nitrogen-rich heterocycles, 1,2,5-oxadiazole stands out for its high positive heat of formation and is extensively used in energetic materials.[6] The 1,3,4-oxadiazole has demonstrated notable applications in a variety of domains, including organic light-emitting diodes (OLEDs), antimicrobial agents, liquid crystals, and photosensitizers. In the field of energetic materials, 1,3,4-oxadiazoles have received increasing attention due to the balanced molecular stability and detonation properties of their derivatives.[7] For instance, 2,5-bis(trinitromethyl)-1,3,4-oxadiazole,[8] a single five-membered heterocyclic compound fully substituted by trinitromethyl group, exhibited acceptable sensitivity; [2,2′-bi(1,3,4-oxadiazole)] 5,5′-dinitramide,[9] not only exhibited commendable thermal stability but also remarkable detonation properties.

The well-known energetic groups typically include the nitro group (–NO$_2$), nitramine (–NHNO$_2$), *gem*-dinitromethyl [–C(NO$_2$)$_2$], *gem*-trinitromethyl [–C(NO$_2$)$_3$], and the amine group (–NH$_2$).[10–12] The energetic materials bearing *gem*-dinitromethyl [–C(NO$_2$)$_2$] and nitramino (–NHNO$_2$) substituents, exhibit high density, favorable oxygen balance, and excellent explosive performance.[13,14] Such compounds have attracted considerable

interest within the realm of energetic materials because of their beneficial characteristics. Furthermore, additional similar compounds have been reported recently, underscoring the versatility and potential of these functional groups in the advancement of high-performance energetic materials.[15–17] Sadly, nitramino-rich compounds show increased susceptibility because the N–NO$_2$ bond has a low dissociation energy.[18,19] The *gem*-dinitromethyl group demonstrates a significant electron-withdrawing effect, typically leading to reduced molecular stability in compounds featuring a single heterocyclic framework with *gem*-dinitromethyl groups.[20] As a result, compounds based on a single heterocycle with nitramine or *gem*-dinitromethyl consistently exhibited poor sensitivity and stability. However, fortunately, the combination of two nitrogen-rich heterocycles substituted with different explosophores was investigated to yield compounds with low sensitivity and good thermal stability.[21–24]

The combination of nitramino, 1,2,5-oxadiazole, *gem*-dinitro methyl, and 1,3,4-oxadiazole moieties was employed in this study to generate novel energetic materials, specifically the neutral species 4-nitramino-3-(5-dinitromethyl-1,3,4-oxadiazol-2-yl)-1,2,5-oxadiazole (**8**) and four corresponding energetic salts. Compound **8** has a higher thermal decomposition temperature than that of *N*,*N*′-([3,3′-bi(1,2,5-oxadiazole)]-4,4′-diyl) dinitramide (**I**)[25] and 2,5-bis(dinitromethyl)-1,3,4-oxadiazole (**II**),[18] while exhibiting similar mechanical sensitivity to 2,5-bis(dinitromethyl)-1,3,4-oxadiazole (**II**) (Fig. 1). Compared to neutral compound **8**, dihydroxylammonium salt (**6**) and dihydrazinium salt (**7**) exhibit similar comparable explosive properties (v_D = 8762 m s^{-1}, P = 33.6 GPa; and

v_D = 8800 m s^{-1}, P = 33.1 GPa, respectively) and enhanced mechanical stability (IS > 40 J, FS > 360 N).

Results and discussion

Synthesis

In this work, the initial compound, 4-amino-3-(5-acetic acid methyl ester-1,3,4-oxadiazol-2-yl)-1,2,5-oxadiazole (**1**), was synthesized following a reported method[26,27] using 4-amino-1,2,5-oxadiazole-3-carbohydrazide as the starting material.[28–30] According to the schematic shown in Scheme 1, when compound **1** was treated with a mixture of 100% HNO$_3$ and 98% H$_2$SO$_4$ at 0 °C, it produced compound **2**, which appeared as a white solid. Subsequent reaction of **2** with ammonia or potassium hydroxide produced the diammonium salt **3** or dipotassium salt **4**, respectively. Due to the formation of unidentified product mixtures during attempts to react **2** with hydroxylamine or hydrazine hydrate, the stable bis-silver salt **5** was synthesized in good yield instead by reacting **3** with silver nitrate. Pure dihydroxylammonium salt **6** and dihydrazinium salt **7** were subsequently obtained *via* metathesis reactions of **5** with hydroxylamine hydrochloride or hydrazine hydrochloride. Finally, the neutral compound, 4-nitramino-3-(5-dinitromethyl-1,3,4-oxadiazol-2-yl)-1,2,5-oxadiazole (**8**), was obtained by acidifying **4** with concentrated sulfuric acid. All the new compounds were characterized by NMR, IR, and DSC. Furthermore, the structures of compounds **3** and **6** were determined by single-crystal X-ray diffraction, and compound **8** was also confirmed by HRMS.


Previous work:

v_D = 9086 m s^{-1}
IS = 1.5 J, FS = 48 N
OB$_{CO}$ = 6.2%
T_d = 80 °C

I
High performance

v_D = 8967 m s^{-1}
IS = 3J, FS = 160N
OB$_{CO}$ = 23%
T_d = 86 °C

II
High oxygen balance
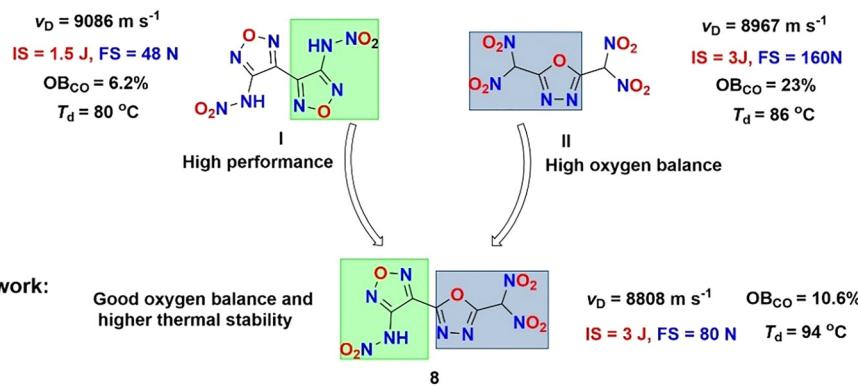
This work:

Good oxygen balance and higher thermal stability

v_D = 8808 m s^{-1} OB$_{CO}$ = 10.6%
IS = 3 J, FS = 80 N T_d = 94 °C

8

2NH$_4$$^+$

2NH$_3$OH$^+$

2N$_2$H$_5$$^+$ v_D = 8501 – 8800 m s^{-1} IS > 40 J, FS > 360 N
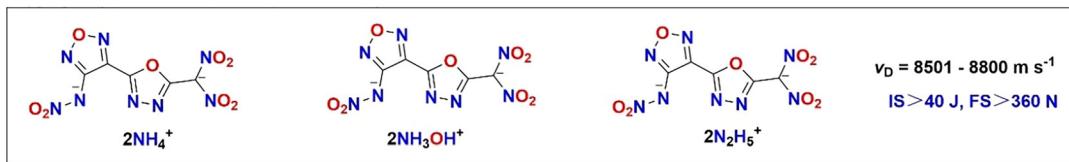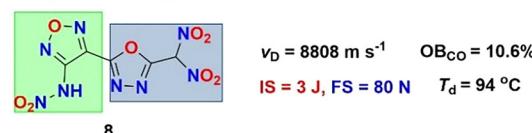
High performance and low sensitivity

Fig. 1   The design of novel energetic compounds.
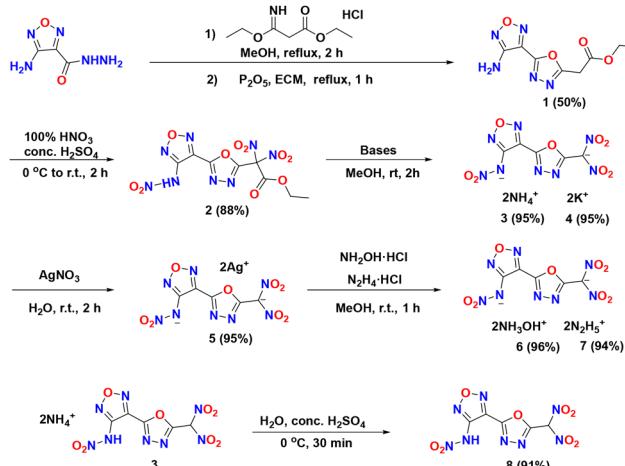
Scheme 1 Synthesis of energetic compounds **1–8**.

X-ray crystallography

Slow vaporization of the compound in H_2O at room temperature yielded crystals of **3** (CCDC 2417137). The molecular structure crystallizes in the triclinic lattice system, specifically within space group $P\bar{1}$. The unit cell contains two molecules and demonstrates a density of 1.834 g cm^{-3} at 301 K. Detailed crystallographic parameters are given in the SI (Tables S1–S7). The 1,2,5-oxadiazole and 1,3,4-oxadiazole rings, along with the *N*-nitro group, are nearly coplanar as evidenced by torsional angles: C2–N6–N10–O2 = $-3.3°$, C2–N6–N10–O6 = 176.0°, and N2–C2–N6–N10 = 0.3°. In contrast, the geminal dinitromethylene groups are slightly twisted relative to the 1,3,4-oxadiazole ring (C4–C3–N1–O4 = $-2.8°$ and C4–C3–N1–O3 = $-27.2°$, Fig. 2a and b). The crystal structure reveals extensive hydrogen bonds (green dotted lines) and exhibits a layered stacking pattern (Fig. 2c and d). With an interplanar distance of 2.87 Å -substantially shorter than the usual aromatic π–π interactions (3.65–4.00 Å),[31] -it indicates that the combination of strong π–π interactions and hydrogen bonding leads to a tightly packed arrangement.
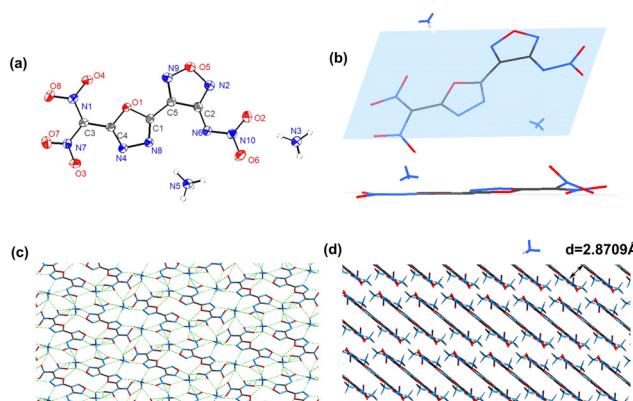
Single crystals of compound **6** (CCDC 2307592), suitable for X-ray diffraction analysis, were cultivated through the controlled evaporation of a MeCN solution at room temperature. This process resulted in the formation of a **6** MeCN solvate. The compound exhibits a monoclinic crystal system, specifically belonging to the $P2_1/n$ space group, and contains four molecules within each unit cell. Its crystal density was measured at 173 K is 1.745 g cm^{-3}. Detailed crystallographic data are provided in Tables S8–S15. The molecular structure (Fig. 3a) shows that the 1,2,5-oxadiazole rings and N-nitro groups are nearly coplanar. In contrast, the rings of 1,3,4-oxadiazole exhibit slight twisting, which is indicated by the torsion angles N2–C2–C3–O2 = 165.6°, N4–N3–C1–N1= $-2.4°$, and N2–C2–C3–O2 = $-11.8°$. A significant torsion angle of 76.2° causes the geminal dinitromethylene group to twist out of the molecular plane (Fig. 3b). The crystal packing of **6** MeCN features a well-defined 3D network sustained by strong hydrogen-bonding interactions, as viewed along the *a*-axis, extended through strong hydrogen bonding interactions (Fig. 3c). Along the *c*-axis, the structure exhibits a wave-like stacking diagram (Fig. 3d).

Theoretical analysis

Hirshfeld surface and fingerprint analysis reveal the "weaknesses" or "stabilization mechanisms" of crystal structures by visualizing the extent of close intermolecular contacts (especially those involving sensitive groups) and quantifying the relative strength and distribution of different types of interactions. Crystal structures with close contacts and a lack of strong stabilizing forces (such as hydrogen bonds or π–π stacking) typically exhibit poor mechanical sensitivity, while structures with effective energy dissipation pathways (strong hydrogen bond networks or extended π systems) and moderate intermolecular voids tend to exhibit good sensitivity. To better understand the intermolecular interactions in crystal **3**, Hirshfeld surface analysis and 2D fingerprint plotting was performed using CrystalExplorer 3.1 (Fig. 4a and b).[32] In these visuals, red


Fig. 2 (a) Crystal structure of **3**; (b) molecular planarity of **3**. (c) A 3D packing diagram along the *a*-axis reveals the arrangement of compound **3**, with green dashed lines indicating hydrogen bonds. (d) Layer-by-layer packing diagram of **3** as observed along the *c*-axis.
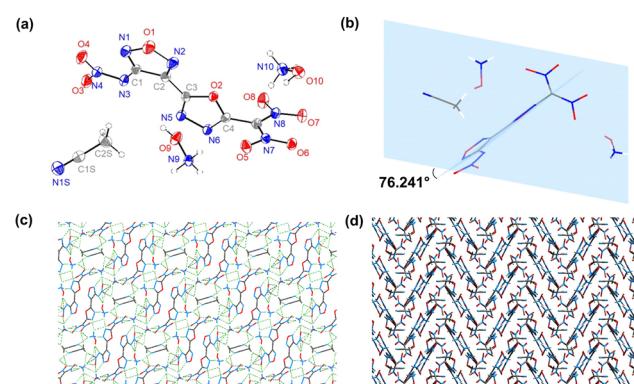
Fig. 3 (a) Crystal structure of **6** MeCN; (b) molecular planarity of 6 MeCN. (c) A 3D packing diagram along the *a*-axis reveals the arrangement of compound **6** MeCN, with green dashed lines indicating hydrogen bonds. (d) An undulating arrangement diagram for the **6** MeCN compound as viewed along the *c*-axis.
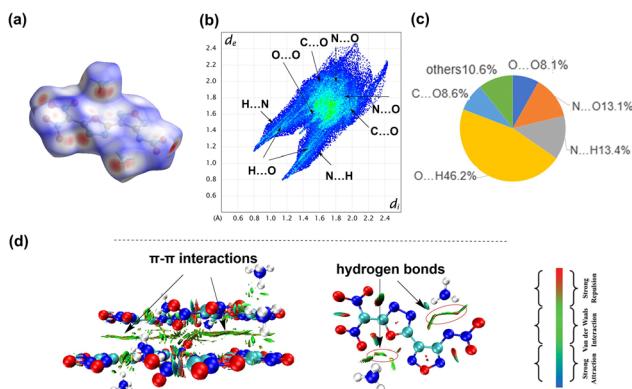
Fig. 4 (a) Hirshfeld surfaces in crystal stacking for **3**. (b) 2D fingerprint plot for **3**. (c) The pie chart for **3** shows the percentage contributions of the individual atomic contacts to the Hirshfeld surface. (d) Noncovalent interaction analysis and π–π interactions for **3** (blue, strong attraction; green, weak attractive interactions; red, strong nonbonded overlap).

and blue areas signify zones of high and low contact density, respectively. The distances from the Hirshfeld surface to the nearest nucleus, both within (di) and outside (de) the surface, create a two-dimensional fingerprint pattern. Fig. 4a emphasizes hydrogen bonding's significant impact on 1,3,4-oxadiazole rings, N-nitro groups, and *gem*-dinitromethylene groups. Fig. 4c quantifies close contacts: O⋯H/H⋯O (46.2%) and N⋯H/H⋯N (13.4%), with interlayer N⋯O (13.1%) and C⋯O (8.6%) contacts attributed to π–π stacking.

Non-covalent interaction (NCI) analysis is also used to determine π–π stacking interactions more intuitively, mainly by analyzing specific color, shape, and location characteristics in its visualization results (commonly referred to as NCI plots).[33] The NCI diagram shows that low electron density gradient (RDG) isosurfaces (typically presented as "dots" or "disks") must be located between the centroids of two or more aromatic rings (such as benzene rings or heteroaromatic rings) or in parallel regions of the ring plane. π–π stacking is primarily driven by dispersion forces, which usually appear as green or blue-green dots in the NCI diagram. Green represents typical weak van der Waals interactions/dispersion forces, which are the main driving force of π–π stacking. If there is a slight additional electrostatic attraction in the π–π stacking (for example, due to the presence of partial charge complementarity), the color may lean slightly towards blue, but green remains the dominant hue. This is significantly different from strong electrostatic interactions, such as hydrogen bonds and ionic bonds, which are depicted as deep blue. Compound **3** exhibits extensive π–π stacking and strong hydrogen bonding (Fig. 4d), which contribute to its enhanced safety properties (IS > 40 J, FS > 360 N) and high density (1.834 g cm^{-3}).

Analysis of the molecular surface electrostatic potential (ESP) and HOMO–LUMO gap provide deeper insights into impact sensitivity. Accordingly, the ESP-mapped van der Waals surface and HOMO–LUMO energy diagram (eV) of compound **3** (IS > 40 J, FS > 360 N) are compared with those of bis(ammonium) 3,3′-dinitramino-4,4′-bifurazane (**IV**) (IS = 10 J, FS = 324 N) and

diammonium 5,5′-dinitromethyl-2,2′-bis(1,3,4-oxadiazolate) (**V**) (IS = 12 J, FS = 180 N).

Strong electrostatic attractions or repulsions between molecules, driven by surface ESP differences, can affect crystal packing, defect formation, and energy transfer efficiency. Areas with high maximum positive values are more likely to form strong electrostatic interaction points, which may become stress concentration points or sites preferential for chemical reactions when subjected to mechanical stimuli, facilitating the formation and triggering of "hot spots". The regions of the molecular surface with the least electron density exhibit a lower degree of "electron deficiency", meaning their ability to attract nucleophiles is weakened. Consequently, the likelihood of forming "hot spots" through electrostatic interactions decreases when external stimuli are applied. This increases the difficulty in inducing strong electronic transfers or disturbances near the bonds, leading to their rupture. As a result, the threshold (energy) required to trigger decomposition or explosion is elevated, and the material exhibits lower sensitivity.[34] As shown in Fig. 5, electrostatic potentials are visualized using color coding. Positive potentials are depicted in red, while negative ones are shown in blue. The maximum and minimum values are localized around the nitro groups and ammonium cations. Compounds **III** and **IV** exhibit maximum positive values of 121.38 kJ mol^{-1} and 153.56 kJ mol^{-1}, respectively. Compound **3** shows a significantly lower value of 110.23 kJ mol^{-1}, suggesting enhanced sensitivity relative to the other compounds.

Molecules with a significant energy gap exhibit a considerable energy difference between their bonding orbitals (like the HOMO) and antibonding orbitals (such as the LUMO). This
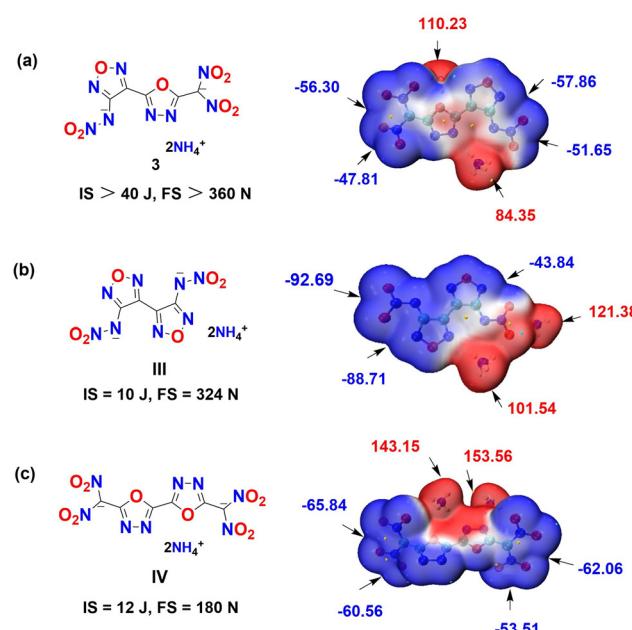

Fig. 5 The ESP-mapped molecular vdW surface for **3** (a), bis(ammonium) 3,3-dinitramino-4,4-bifurazane (b) and diammonium 5,5′-dinitromethyl-2,2′-bis(1,3,4-oxadiazolate) (c).
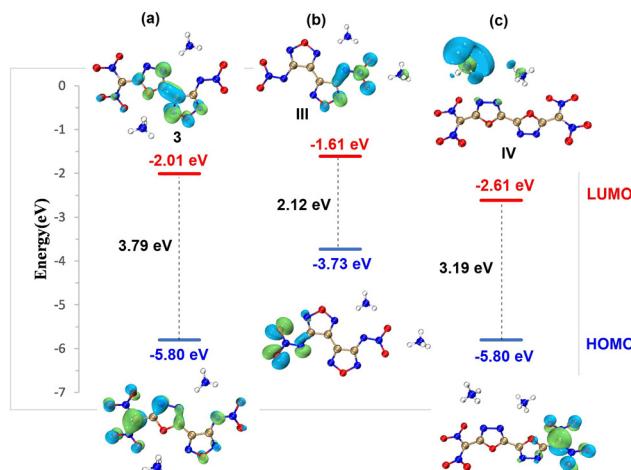
Fig. 6 HOMO–LUMO energy (in eV) level maps of compounds **3** (a), bis(ammonium) 3,3-dinitramino-4,4-bifurazane (b) and diammonium 5,5′-dinitromethyl-2,2′-bis(1,3,4-oxadiazolate) (c).

typically indicates that the bonding electrons are more tightly bound, the bonds are stronger, and the overall energy of the molecule is lower, rendering it relatively more stable.[35] As shown in Fig. 6, compound **3** exhibits a lower calculated HOMO energy level (-5.80 eV) than **III** (-3.73 eV) and a higher LUMO energy level (-2.01 eV) than **IV** (-2.61 eV). It also possesses the largest HOMO–LUMO gap (3.79 eV). These results effectively explain the greater mechanical stability of compound **3** compared to dinitramine- and dinitromethyl-based ammonium salts **III** and **IV**.

Physical and detonation properties

The densities of the newly synthesized compounds vary from 1.79 to 2.05 g cm^{-3}. These values were determined using a gas pycnometer at an ambient temperature of 25 °C. To assess their thermal stability, differential scanning calorimetry (DSC) was employed, conducted under a flow of nitrogen at a heating rate of 5 °C per minute. The outcomes of these analyses are compiled and presented in Fig. S2 through S8. The neutral compound **8** exhibits low thermal stability ($T_{\text{dec}} = 94$ °C, onset). Ionic compounds **3–5** and **7** show higher thermal stabilities of 187.8 °C, 241 °C, 167 °C and 156 °C (onset), respectively, which indicates the superiority of saltation strategy in terms of

enhancing molecular stability. The heats of formation ($\Delta_f H$) for these compounds were determined using Gaussian 16 computational software.[36]

By incorporating these computed $\Delta_f H$ values alongside experimentally determined densities, the detonation velocity and pressure were evaluated through the use of the EXPLO5 software, specifically version 6.05.[37] As illustrated in Table 1, the physiochemical properties of compounds **3**, **4**, and **6–8** were compared with traditional explosives TNT[38] and RDX.[39] The detonation properties of **3** (8501 m s^{-1}, 30.0 GPa) and **4** (7739 m s^{-1}, 26.0 GPa) are superior to those of TNT (6881 m s^{-1}, 19.5 GPa), respectively. Compounds **6-8** exhibit calculated detonation properties (**6**, 8762 m s^{-1}, 33.6 GPa; **7**, 8800 m s^{-1}, 33.1 GPa; **8**, 8808 m s^{-1}, 34.2 GPa) similar to RDX (8795 m s^{-1}, 34.9 GPa). For safety assessment, impact and friction sensitivities were measured using standard BAM methodologies. Compound **8** has a high impact sensitivity (3 J), while compound **4** exhibits acceptable sensitivity (9 J, 160 N). In contrast, compounds **3**, **6**, and **7** are classified as insensitive due to their impact sensitivities exceeding 40 J and friction sensitivities surpassing 360 N.

Conclusions

In summary, this study successfully designed and synthesized a novel neutral energetic compound, 4-nitramino-3-(5- dinitro methyl-1,3,4-oxadiazol-2-yl)-1,2,5-oxadiazole (**8**), along with its four energetic salts (diammonium **3**, dipotassium **4**, dihydroxylammonium **6**, and dihydrazinium **7**) by strategically combining the high-energy-density building blocks nitramino (-NHNO$_2$), gem-dinitromethyl [–C(NO$_2$)$_2$], 1,2,5-oxadiazole, and 1,3,4-oxadiazole. A comprehensive characterisation of their structures was conducted, and the structures of **3** and **6** were further determined by single crystal X-ray diffraction. Crystallographic and Hirshfeld surface analyses show that extensive hydrogen-bonding networks, strong π–π stacking interactions (evidenced by short interplanar distances ∼2.87 Å in **3**), and optimized molecular surface electrostatic potentials (lower maximum positive ESP value relative to sensitive analogues **III** and **IV**) and HOMO–LUMO gaps (larger gap for **3**) are critical factors contributing to the high density, thermal stability, and low sensitivity observed in the ammonium salt **3**. Neutral compound **8** shows high impact sensitivity (3 J) and friction sensitivity (80 N), as well as high explosive performance of 8808 m s^{-1} and 34.2 GPa. Based on the DSC results, the

Table 1   Properties of energetic compounds **7-12**

Comp.	$T_d{}^a$ (°C)	ρ^b (g cm^{-3})	$\Delta_f H^c$ (kJ mol^{-1}/kJ g^{-1})	N^d (%)	$\nu_D{}^e$ (m s^{-1})	P^f (GPa)	IS^g (J)	FS^h (N)	$\Omega_{\text{CO}}{}^i$ (%)
3	188	1.81	29.7/0.09	41.39	8501	30.0	>40	>360	−4.76
4	241	2.05	−290.5/−0.77	29.65	7739	26.0	9	160	12.7
6	167	1.80	160.7/0.44	37.38	8762	33.6	>40	360	4.35
7	156	1.79	311.1/0.85	45.46	8800	33.1	>40	360	−8.74
8	94	1.79	388.5/1.29	35.71	8808	34.2	3	80	10.6
TNT	295	1.65	−59.3/−0.26	18.5	6881	19.5	15	360	−24.7
RDX	204	1.80	70.3/0.36	37.8	8795	34.9	7.4	120	0

^{a} Decomposition temperature (onset) under nitrogen (DSC, 5 °C min^{-1}). ^{b} Density measured by gas pycnometer (25 °C). ^{c} Heat of formation. ^{d} Nitrogen content. ^{e} Detonation velocity (calculated with Explo5 6.05). ^{f} Detonation pressure (calculated with Explo5 v6.05). ^{g} Impact sensitivity. ^{h} Friction sensitivity. ^{i} Oxygen balances for C$_a$H$_b$O$_c$N$_d$, 1600(c−a−b/2)/M_W; M_W = Molecular weight – based on CO formation.

decomposition temperatures of the salts (**3–7**) are in the range of 156 to 241 °C. Furthermore, compared to TNT and RDX, the salts (**3**, **6** and **7**) show better sensitivities towards impact and friction. Additionally, compounds **6** and **7** have excellent calculated detonation properties (**6**, 8759 m s^{-1}, 33.6 GPa; **7**, 8800 m s^{-1}, 33.1 GPa), which are comparable to those of RDX, showing great promise as replacements.

Conflicts of interest

There are no conflicts to declare.

Data availability

All data relevant to the work described here are available in the supplementary information (SI). All other relevant data generated an analysed during this study, which include experimental, spectroscopic, crystallographic and computational data, are included in the supplementary information. See DOI: **https://doi.org/10.1039/d5ma00829h**.

Acknowledgements

Notes and references

1 N. Fischer, D. Fischer, T. M. Klapötke, D. G. Piercey and J. Stierstorfer, *J. Mater. Chem. A*, 2012, **22**, 20418–20422.
2 C. He, Y. Tang, L. A. Mitchell, D. A. Parrish and J. M. Shreeve, *J. Mater. Chem. A*, 2016, **4**, 8969–8973.
3 Y. Peng, Q. Yu and W. Yi, *ACS Appl. Mater. Interfaces*, 2024, **16**, 63419–63426.
4 Q. Yu, Z. Zheng, Z. Yi, W. Yi and J. M. Shreeve, *J. Am. Chem. Soc.*, 2025, **147**, 5125–5131.
5 H. Gao and J. M. Shreeve, *Chem. Rev.*, 2011, **111**, 7377–7436.
6 A. B. Sheremetev, E. A. Ivanova, N. P. Spiridonova, S. F. Melnikova, I. V. Tselinsky, K. Y. Suponitsky and M. Y. Antipin, *J. Heterocycl. Chem.*, 2005, **42**, 1237–1242.
7 M. A. Kettner, K. Karaghiosoff, T. M. Klapötke, M. Sućeska and S. Wunder, *Chem. – Eur. J.*, 2014, **20**, 7622–7631.
8 D. Fischer, T. M. Klapötke and J. Stierstorfer, *Chem. – Eur. J.*, 2016, **22**, 4966–4970.
9 W. Zhang, J. Zhang, M. Deng, X. Qi, F. Nie and Q. A. Zhang, *Nat. Commun.*, 2017, **8**, 181.
10 S. Banik, P. Kumar, V. D. Ghule, S. Khanna, D. Allimuthu and S. Dharavath, *J. Mater. Chem. A*, 2022, **10**, 22803–22811.
11 Y. Hu, W. Dong, Z. Lu, H. Zhang and J. Zhang, *Chem. Commun.*, 2023, **59**, 9864–9867.
12 Q. Yu, F. Li, P. Yin, S. Pang, R. J. Staples and J. M. Shreeve, *J. Mater. Chem. A*, 2021, **9**, 24903–24908.
13 H. Huang, Y. Li, J. Yang, R. Pan and X. Lin, *New J. Chem.*, 2017, **41**, 7697–7704.
14 Y. Tang, S. Dharavath, G. H. Imler, D. A. Parrish and J. M. Shreeve, *Chem. – Eur. J.*, 2017, **23**, 9185–9191.
15 Y. Cao, H. Huang, X. Lin, J. Yang and X. Gong, *New J. Chem.*, 2018, **42**, 11390–11395.
16 J. Zhang, S. Dharavath, L. A. Mitchell, D. A. Parrish and J. M. Shreeve, *J. Am. Chem. Soc.*, 2016, **138**, 7500–7503.
17 Y. Chen, Q. Yu, N. Liu, T. Li and W. Yi, *J. Org. Chem.*, 2024, **89**, 17475–17481.
18 D. Fischer, T. M. Klapötke and J. Stierstorfer, *Angew. Chem., Int. Ed.*, 2015, **54**, 10299–10302.
19 Y. Tang, J. Zhang, L. A. Mitchell, D. A. Parrish and J. M. Shreeve, *J. Am. Chem. Soc.*, 2015, **137**, 15984–15987.
20 Q. Yu, P. Yin, J. Zhang, C. He, G. H. Imler, D. A. Parrish and J. M. Shreeve, *J. Am. Chem. Soc.*, 2017, **139**, 8816–8819.
21 D. Kumar, C. He, L. A. Mitchell, D. A. Parrish and J. M. Shreeve, *J. Mater. Chem. A*, 2016, **4**, 9220–9228.
22 D. Kumar, L. A. Mitchell, D. A. Parrish and J. M. Shreeve, *J. Mater. Chem. A*, 2016, **4**, 9931–9940.
23 C. He, G. H. Imler, D. A. Parrish and J. M. Shreeve, *J. Mater. Chem. A*, 2018, **6**, 16833–16837.
24 J. Ma, J. Tang, H. Yang, Z. Yi, G. Wu, S. Zhu, W. Zhang, Y. Li and G. Cheng, *ACS Appl. Mater. Interfaces*, 2019, **11**, 26053–26059.
25 D. Fischer, T. M. Klapötke, M. Reymann and J. Stierstorfer, *Chem. – Eur. J.*, 2014, **20**, 6401–6411.
26 V. V. Kiseleva, A. A. Gakh and A. A. Fainzilberg, *Russ. Chem. Bull.*, 1990, **39**, 1888–1895.
27 J. Tian, H. Xiong, Q. Lin, G. Cheng and H. Yang, *New J. Chem.*, 2017, **41**, 1918–1924.
28 J. L. Catrow, Y. Zhang, M. Zhang and H. Ji, *J. Med. Chem.*, 2015, **58**, 4678–9462.
29 A. O. Finogenov, A. S. Kulikov, M. A. Epishina, I. V. Ovchinnikov, Y. V. Nelyubina and N. N. Makhova, *J. Heterocycl. Chem.*, 2013, **50**, 135–410.
30 A. S. Kulikov, I. V. Ovchinnikov, S. I. Molotov and N. N. Makhova, *Russ. Chem. Bull.*, 2003, **52**, 1822–1828.
31 H. D. B. Jenkins, D. Tudela and L. Glasser, *Inorg. Chem.*, 2002, **41**, 2364–2367.
32 M. A. Spackman and D. Jayatilaka, *CrystEngComm*, 2009, **11**, 19–32.
33 E. R. Johnson, S. Keinan, P. Mori-Sánchez, J. Contreras-García, A. J. Cohen and W. Yang, *J. Am. Chem. Soc.*, 2010, **132**, 6498–6506.
34 W. Humphrey, A. Dalke and K. Schulten, *J. Mol. Graphics*, 1996, **14**, 33–38.
35 T. Lu and F. Chen, *J. Comput. Chem.*, 2012, **33**, 580–592.
36 M. J. Frisch, G. W. Trucks, H. B. Schlegel, G. E. Scuseria, M. A. Robb and J. R. Cheeseman, *et al. Gaussian 16 Rev. B.01*. Gaussian, Inc., Wallingford CT, 2016.
37 M. Suceska, EXPLO5 6.05. Brodarski Institute, Zagreb, Croatia, 2020.
38 A. K. Yadav, V. D. Ghule and S. Dharavath, *Mater. Chem. Front.*, 2021, **5**, 8352–8360.
39 J. Tang, H. Xiong, G. Zhang, Y. Tang, H. Yang and G. Cheng, *Chem. Commun.*, 2022, **58**, 11847–11850.